Hindawi Publishing Corporation
International Journal of Photoenergy
Volume 2013, Article ID 416245, 7 pages
http://dx.doi.org/10.1155/2013/416245

Research Article

The Effect of Annealing Temperature and KCN Etching on the Photovoltaic Properties of $Cu(In,Ga)(S,Se)_2$ Solar Cells Using Nanoparticles

Duy-Cuong Nguyen,[1,2] Ken Fukatsu,[1] Keiji Tanimoto,[1] Shigeru Ikeda,[3] Michio Matsumura,[3] and Seigo Ito[1]

[1] *Department of Electrical Engineering and Computer Sciences, Graduate School of Engineering, University of Hyogo, 2167 Shosha, Himeji, Hyogo 671-2280, Japan*
[2] *Advanced Institute for Science and Technology, Hanoi University of Science and Technology, No 1, Dai Co Viet Rd., Hai Ba Trung, Hanoi, Vietnam*
[3] *Research Center for Solar Energy Chemistry, Osaka University, Toyonaka 560-8531, Japan*

Correspondence should be addressed to Seigo Ito; itou@eng.u-hyogo.ac.jp

Received 16 March 2013; Revised 14 May 2013; Accepted 15 May 2013

Academic Editor: Mingce Long

$Cu(In,Ga)S_2$ nanoparticles were synthesized by a hot-injection method under a low-vacuum ambience, which were printed and annealed with Se vapor for $Cu(In,Ga)(S,Se)_2$ solar cells. The $Cu(In,Ga)S_2$ nanoparticles were around 14 nm, and the stable ink was obtained by dispersing the nanoparticles in hexanethiol. The crystallinity of the $Cu(In,Ga)(S,Se)_2$ films increased with the increase in annealing temperature. $Cu(In,Ga)(S,Se)_2$ solar cells with KCN etching after annealing showed better photovoltaic properties than KCN etching before annealing and without etching. The best cell was observed at an annealing temperature of 540°C and KCN etching after annealing; the parameters of this cell were a short-circuit photocurrent density of 27.12 mA/cm^2, open-circuit voltage of 0.42 V, fill factor of 0.38, and conversion efficiency of 4.3%.

1. Introduction

$Cu(In,Ga)(Se,S)_2$ (CIGS) solar cells have received the consideration of many researchers around the world because of their attractive properties: high stability and efficiency, and the diversity of fabricating methods including both vacuum and nonvacuum methods such as coevaporation, sputtering, printing, and spin coating [1–6]. The durability and efficiency of CIGS solar cells are higher than those of the other printed solar cells, such as polymer and dye-sensitized solar cells. The fabrication method of CIGS solar cells is more multiform than silicon solar cells. The record conversion efficiency of CIGS solar cells was 20.3% on the glass substrate with Mo as a back contact and 20.4% on polymer flexible substrates; these solar cells were prepared by the vacuum methods [7, 8]. Recently, the CIGS solar cells fabricated by nonvacuum methods, such as printing and spin coating using CIGS nanoparticles or a solution, have been developing widely [9–14]. Although the conversion efficiency of non-vacuum-processed CIGS solar cells was lower than that of vacuum-processed CIGS solar cells, the non-vacuum methods are quite attractive because they are a simple and high-speed process. In addition, the production setup can be cost effective. For these reasons, they are expected to be low-cost solar cells in the future. Among the non-vacuum methods, the authors were interested in the printing method because it is able to fabricate large-scale samples quickly. Todorov et al. obtained a conversion efficiency of 15.2% with CIGS solar cells fabricated by the solution process using a hydrazine solvent; however, the hydrazine was highly toxic for the mass production of photovoltaic cells [15]. Without the hydrazine method, Guo et al. showed a 12% conversion efficiency by printing CIGS nanoparticles with several KCN etchings before annealing [13]. In this paper, we have fabricated the solar cells from

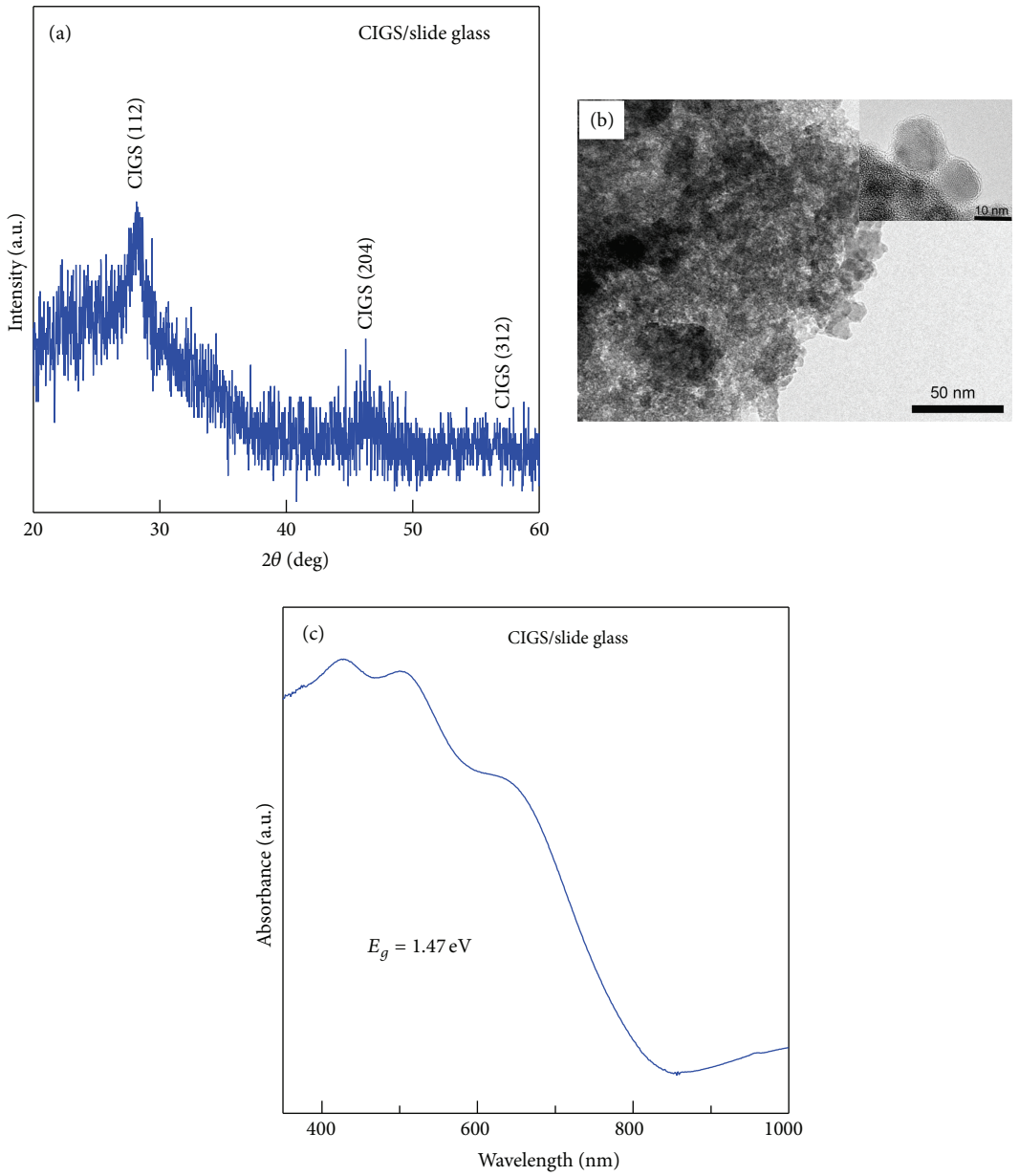

Figure 1: XRD pattern (a) and absorption spectrum (c) of CIGS nanoparticles coated on slide glass and TEM images of CIGS nanoparticles (b). The inset in (b) is a high-magnification TEM image of CIGS nanoparticles.

CIGS nanoparticles and analyzed the effect of the annealing temperature and the KCN etching before and after annealing the CIGS layers.

2. Experimental

The CIGS nanoparticles were prepared by a hot-injection method [16, 17]. Copper (II) acetylacetonate (purity > 97%, Tokyo Chemical), indium (III) acetylacetonate (purity > 97%, Tokyo Chemical), gallium (III) acetylacetonate (purity of 99.99%, Aldrich), and sulfur powder (purity of 99%, Kishida) were chosen for copper, indium, gallium, and sulfur precursors to synthesize CIGS nanoparticles.

Firstly, precursors of 0.785 g of Cu, 0.865 g of In, and 0.33 g of Ga corresponding with the atomic ratio of Cu : In : Ga = 1 : 0.7 : 0.3 were mixed with a 15 mL oleylamine solvent (>40%, Tokyo Chemical) in a trinecked flask under magnetic stirring, then heated up to 130°C and kept at this temperature for 30 min. Before heating the mixture, nitrogen gas was inserted into the flask and then removed by a rotary pump for the purpose of purging oxygen. During heating and reaction the ambience inside the flask was kept at a low vacuum, and was not pumped further. Secondly, temperature was increased to 250°C, and a 9 mL solution of 1 M sulfur that was dissolved in oleylamine was injected; after injection, the temperature was kept at 250°C for 30 min to complete

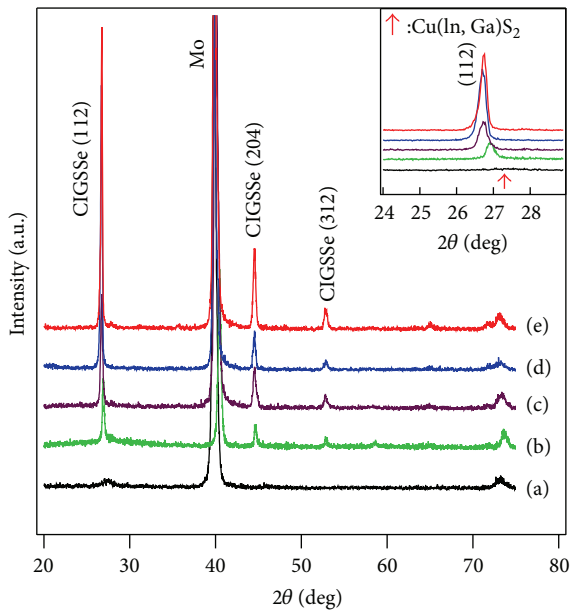

FIGURE 2: XRD pattern of CIGS/Mo without (a) and with annealing at temperatures of 500 (b), 520 (c), 540 (d), and 560°C (e) for 30 min under a selenium vapor ambience. The inset shows the x-axis magnified peaks from 24° to 30°. The arrow is the position of $Cu(In,Ga)S_2$ (112) [16].

the reaction. After that, the solution was cooled down to 60°C, which included the CIGS nanoparticles, the excess of sulfur, and the solvent. In order to separate the CIGS nanoparticles from subsidiary materials, the solution was mixed with hexane and isopropanol, and then centrifuged at 3400 rotations per minute for 15 min. This washing cycle was repeated three times. The volumes of mixed solvent of hexane and isopropanol were 8 mL/40 mL, 4 mL/44 mL, and 2 mL/46 mL for the first, second, and third times, respectively. After separating, the CIGS nanoparticles were dried under a nitrogen flow at room temperature. Finally, the CIGS nanoparticles were dispersed in a hexanethiol solvent to form a stable ink. Also, CIGS nanoparticles were dispersed in a toluene solvent; however, this ink was unstable and easily solidified after several weeks. We tried to measure the composition of the final powder by EDX combined in TEM system. However, it is difficult to obtain the consensus results using the CIGS nanopowder, which may be due to the segregation in the CIGS colloidal solution.

The structure of CIGS solar cells was Ag/Al-doped ZnO/ZnO/CdS/CIGS/Mo/glass substrate. To fabricate CIGS cells, CIGS films with a thickness of 700–800 nm were printed on Mo/glass substrates by a doctor blade method. CIGS films were annealed at various temperatures in a graphite box with 0.2 g of Se powder to make high crystallinity CIGS films. In order to investigate the effect of KCN etching on the photovoltaic property, CIGS films were etched for 2 min before or after annealing in a 0.5 M KCN solution. A 50 nm CdS layer was deposited by the chemical bath deposition method (CBD). 50 nm ZnO and 400 nm Al-doped ZnO window layers were deposited by RF-magnetron sputtering at 50 W and 100 W, respectively; these films were deposited at room temperature and at a pressure of 0.5 Pa. Then, the samples were heated at 200°C for 6 h under an air ambience before completing cell with Ag electrodes using an Ag paste. The device heated at 200°C showed a significant increase in cell parameters such as J_{SC}, V_{OC}, and FF in comparison with without heating. The increase of cell performance may be due to the improvement of the connection between layers. The area of cells for the photocurrent density-voltage (J-V) measurement is $0.5 \times 0.5\,cm^2$.

The microstructure and film thickness of CIGS were viewed by scanning electron microscopy (SEM) (JSM-6510, JEOL). The crystallinity and preferred orientation of CIGS films were confirmed by X-ray diffraction (XRD) (MiniFlex II, Rigaku). The particle sizes of the CIGS nanoparticles were determined by the high-resolution transmission electron microscopy (HRTEM; JEM 2100F). Absorption spectra were measured by an ultraviolet-visible spectroscopy (Lambda 750 UV/VIS Spectrometer, Perkin Elmer). Photovoltaic measurements employed an AM 1.5 solar simulator equipped with a xenon lamp (YSS-100A, Yamashita Denso, Japan). The power of the simulated light was calibrated to 100 mW cm^{-2} by using a reference Si photodiode (Bunkou Keiki, Japan). I-V curves were obtained by applying an external bias to the cell and measuring the generated photocurrent with a DC voltage current source (6240, ADCMT).

3. Results and Discussion

Figure 1 shows the XRD pattern, TEM image, and absorption spectrum of CIGS nanoparticles being synthesized at 250°C under a low-vacuum ambience. X-ray diffraction weak points were observed at the positions of 28.14, 46.28, and 56.70°; these peaks of CIGS were indexed as (112), (204), and (312), respectively [18]. From the XRD pattern, the second phase was not observed in the powder. In order to calculate the crystallite size, the Scherrer equation was applied:

$$d = \frac{0.9\lambda}{B\cos(\theta)}, \quad (1)$$

where d is the average crystallite size, λ is the wavelength used (0.15405 nm), B is the width at mean height of the diffraction peak, and θ is the angle of diffraction. The average crystallite size of CIGS nanoparticles with the preferred orientation of (112) was 12 nm. To better confirm CIGS nanoparticle size, high-resolution TEM measurement was performed and the result was shown in Figure 1(b). The particle size obtained from TEM data was around 14 nm. This result is quite close to the crystallite size being calculated from XRD data as discussed previously. Figure 1(c) shows the absorption spectrum of CIGS coating on slide glass. The absorption edge was observed at 843 nm; the band gap calculated from absorption spectrum is 1.47 eV.

The XRD pattern of CIGS films without annealing and with annealing at 500, 520, 540, and 560°C for 30 min under selenium vapor ambience is shown in Figure 2. The peak position of the annealed samples shifted towards the lower angle of diffraction in comparison with the sample without

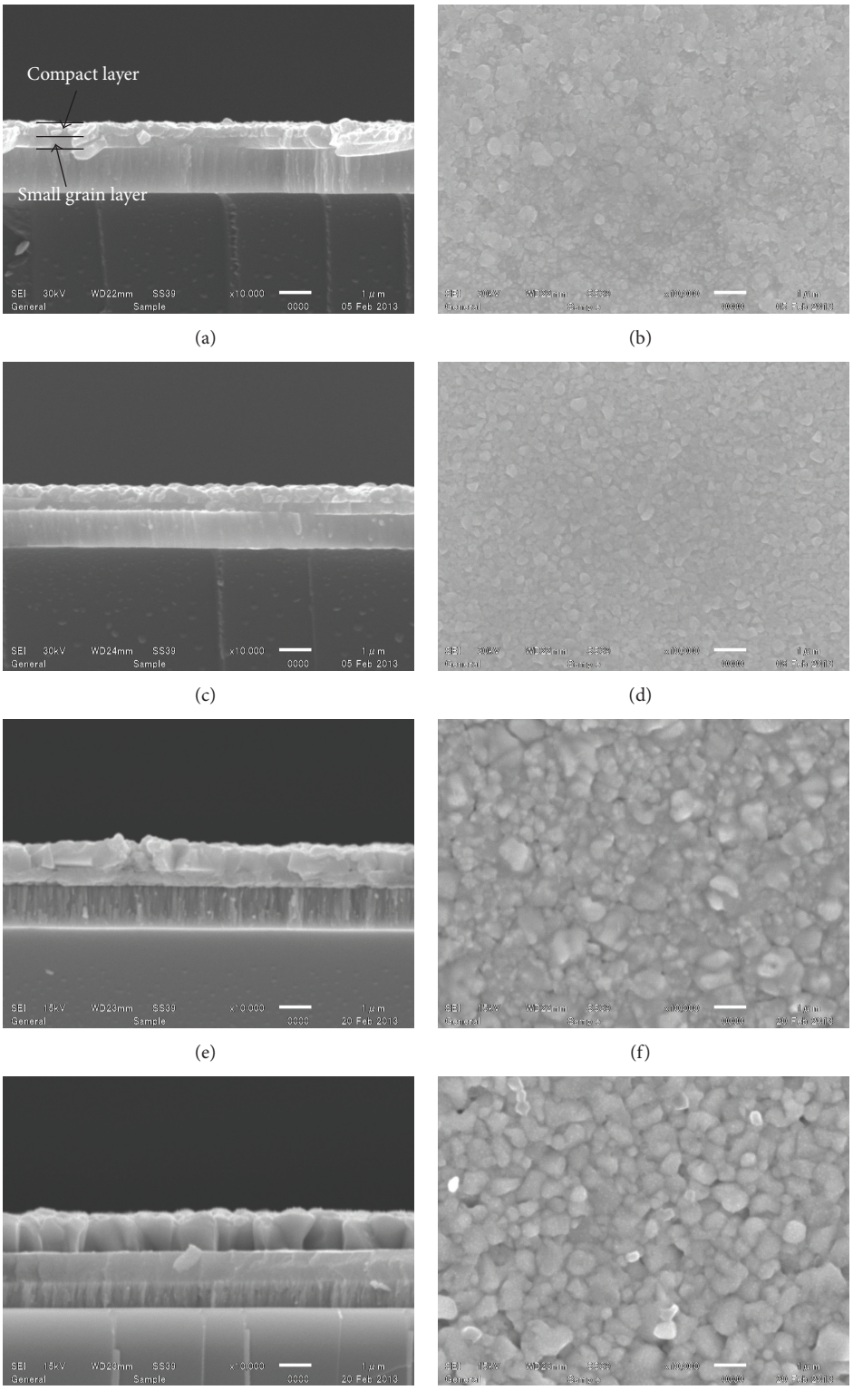

Figure 3: Cross-sectional and surface SEM images of CIGS films annealed at temperatures of 500 ((a), (b)), 520 ((c), (d)), 540 ((e), (f)), and 560°C ((g), (h)) for 30 min under a selenium vapor ambience.

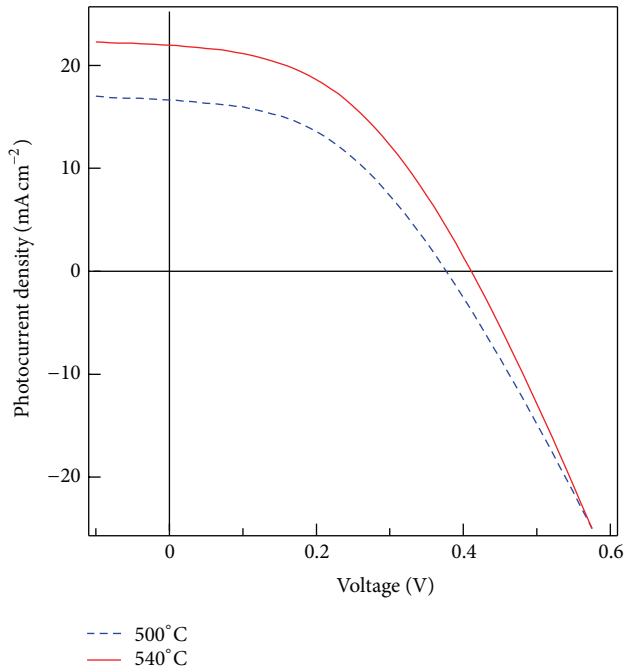

Figure 4: Photocurrent density-voltage curves of CIGS solar cells annealing at 500 and 540°C for 30 min under a selenium vapor ambience.

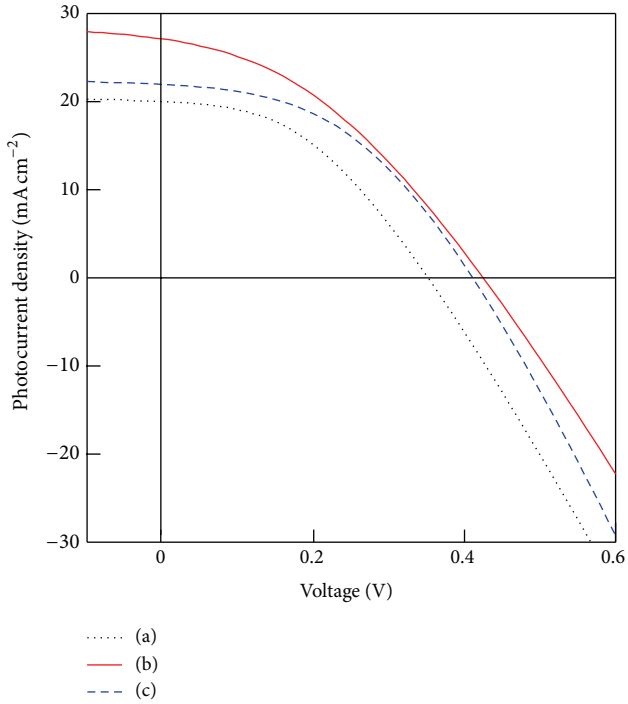

Figure 5: Photocurrent density-voltage curves of CIGS solar cells with KCN etching before annealing (a), after annealing (b), and without KCN etching (c); all samples annealed at 540°C for 30 min under selenium vapor ambience.

annealing; this phenomenon can be clearly viewed in the case of peak (112) as shown in the inset of Figure 2. The red arrow in the inset shows the position of the CIGS peak without annealing. The shift in XRD peaks is due to the replacement of sulfur by selenium in CIGS films. The direction of the peak shift toward lower diffraction angle is attributed to the ion radius (191 pm for −2e) being bigger than sulfur (184 pm for −2e). In addition, the XRD peak intensely increased with the increase in annealing temperature. This indicates that the crystallinity of CIGS films is better at

higher annealing temperatures. Peak intensity of the films annealed at 500 and 520°C was not very high; however, it drastically increased at the sample annealing at 540 and 560°C. The increase of the crystallinity is partly the increase of selenium concentration in CIGS films. The authors tried to anneal CIGS films under sulfur vapor ambience; however, the crystallinity insignificantly improved. The crystallinity of CIGS films strongly affects the photovoltaic properties.

In order to analyze the microstructural properties of CIGS films, an SEM observation was carried out. Figure 3 shows the cross-sectional and surface SEM image of CIGS annealing at 500, 520, 540, and 560°C for 30 min under a selenium vapor ambience. From the cross-sectional images, two layers were observed in all samples and these layers were described as compact and small grain layers in Figure 3(a). The compact (high crystallinity) and small grain (low crystallinity) layers are thicker and thinner at higher annealing temperatures, respectively. The small grain layer may contain carbon which is generated from solvents in the CIGS ink [19, 20]. The surface of the samples annealed at 500 and 520°C showed small CIGS crystal particles. The crystallites rose with the increase of annealing temperature, resulting in an improvement of the crystallinity in CIGS films as shown in the XRD pattern. Big crystal particles were observed at the sample annealed at 540 and 560°C.

Figure 4 shows the photocurrent density-voltage curve of CIGS solar cells annealed at 500 and 540°C. The cell performance of the sample annealed at 540°C was better than that of the sample annealed at 500°C. Photovoltaic parameters of CIGS solar cells annealed at 500°C were short-circuit photocurrent density (J_{SC}) = 16.64 mA cm^{-2}, open-circuit voltage (V_{OC}) = 0.38 V, fill factor (FF) = 0.45, and conversion efficiency (η) = 2.79%. The photovoltaic parameters were improved by annealing at a higher temperature (540°C) as J_{SC} = 21.96 mA/cm^2, V_{OC} = 0.41 V, FF = 0.44, and η = 4.01%. The better cell performance of the sample annealed at 540°C compared to the other one annealing at 500°C was attributed to the higher crystallinity as confirmed by XRD and SEM. V_{OC} and FF of these cells are lower than those by vacuum deposition methods [1, 7, 8]; the reason may be due to the existence of the small grain layer containing carbon as shown in the SEM cross-section images in Figure 3.

In order to investigate the effect of KCN etching on cell performance, CIGSS films were etched before and after annealing by a 0.5 M KCN solution for 2 min. The photocurrent-voltage curves of the sample with and without etching are shown in Figure 5. The best cell was observed in the sample with a 2 min KCN etching after annealing; the cell parameters of that one were J_{SC} = 27.12 mA/cm^2, V_{OC} = 0.42 V, FF = 0.38, and η = 4.3%.

The KCN treatment has been utilized to remove Cu-rich layers ($CuSe_x$ or CuS_x) and to improve the crystallinity of CIGS and CIS [21–25]. Guo et al. reported 12% efficiency in printed-CIGS solar cells using several KCN treatments before annealing [13]. The effect of several KCN treatments on printed CIGS looks not only for the etching of Cu-rich layer, but also for the removal of carbon contamination from hexanethiol, resulting in high crystallinity CIGS layer. Without such carbon removal by the repeated CIGS coatings and low-temperature annealings (at 300°C), the carbon-rich layer aroused [19, 20]. The resulting CIGS layer is divided into two parts of pure CIGS and carbon-rich CIGS as Figures 3(a) and 3(c) show. In this work, although the KCN treatment before annealing deteriorated the photovoltaic results, the KCN treatment after annealing enhanced the J_{SC}, which may work for further studies. Although the morphology and microstructures of the CIGSS films after etching should be provided for comparison, the data was not obtained at this time and should be provided in the future.

4. Conclusions

The CIGS nanoparticles were successfully synthesized by the hot-injection method. The crystallinity of CIGS films increased with the increase of annealing temperature. Compacted and small grain layers were observed in all samples annealed at temperatures in the range of 500–560°C. In the case of different annealing temperatures, the sample annealed at 540°C showed the best cell performance. The parameters of the best cell annealed at 540°C with a 2 min KCN etching and after annealing were J_{SC} = 27.12 mA/cm^2, V_{OC} = 0.42 V, FF = 0.38, and η = 4.3%. In order to get better cell performance, the small grain layer should be converted into a compact layer in the cells.

References

[1] I. Repins, M. A. Contreras, B. Egaas et al., "19.9%-efficient ZnO/CdS/CuInGaSe$_2$ solar cell with 81.2% fill factor," *Progress in Photovoltaics: Research and Applications*, vol. 16, no. 3, pp. 235–239, 2008.

[2] J. H. Shi, Z. Q. Li, D. W. Zhang, Q. Q. Liu, Z. Z. Sun, and S. M. Huang, "Fabrication of Cu(In, Ga)Se$_2$ thin films by sputtering from a single quaternary chalcogenide target," *Progress in Photovoltaics: Research and Applications*, vol. 19, no. 2, pp. 160–164, 2011.

[3] D. B. Mitzi, M. Yuan, W. Liu et al., "A high-efficiency solution-deposited thin-film photovoltaic device," *Advanced Materials*, vol. 20, no. 19, pp. 3657–3662, 2008.

[4] T. Wada, Y. Matsuo, S. Nomura et al., "Fabrication of Cu(In,Ga)Se$_2$ thin films by a combination of mechanochemical and screen-printing/sintering processes," *Physica Status Solidi (A)*, vol. 203, no. 11, pp. 2593–2597, 2006.

[5] B. S. Ko, S. J. Sung, D. H. Kim, D. H. Lee, and D. K. Hwang, "Effects of annealing on structural and electrical properties of sub-micron thick CIGS films," *Current Applied Physics*, 2013.

[6] H. C. Wang, C. C. Wang, S. W. Feng, L. H. Chen, and Y. S. Lin, "Synthesis of CIGS thin film by solvothermal route," *Optical Materials Express*, vol. 3, pp. 54–66, 2013.

[7] P. Jackson, D. Hriskos, E. Lotter et al., "New world record efficiency for Cu(In, Ga)Se$_2$ thin film solar cells beyond 20%," *Progress in Photovoltaics: Research and Applications*, vol. 19, no. 7, pp. 894–897, 2011.

[8] P. Bloesch, A. Chirila, P. Reinhard, S. Nishiwaki, S. Buecheler, and A. N. Tiwari, "Electrical back contact and impurities in CIGS solar cells," in *Proceedings of the 5th International Symposium on Innovative Solar Cells*, Tsukuba, Japan, January, 2013.

[9] V. K. Kapur, A. Bansal, P. Le, and O. I. Asensio, "Non-vacuum processing of $CuIn_{1-x}GaxSe_2$ solar cells on rigid and flexible substrates using nanoparticle precursor inks," *Thin Solid Films*, vol. 431-432, pp. 53–57, 2003.

[10] V. A. Akhavan, B. W. Goodfellow, M. G. Panthani et al., "Colloidal CIGS and CZTS nanocrystals: a precursor route to printed photovoltaics," *Journal of Solid State Chemistry*, vol. 189, pp. 2–12, 2012.

[11] A. R. Uhl, Y. E. Romanyuk, and A. N. Tiwari, "Thin film $Cu(In,Ga)Se_2$ solar cells processed from solution pastes with polymethyl methacrylate binder," *Thin Solid Films*, vol. 519, no. 21, pp. 7259–7263, 2011.

[12] S. J. Park, J. W. Cho, J. K. Lee, K. Shin, J. H. Kim, and B. K. Min, "Solution processed high band-gap $CuInGaS_2$ thin film for solar cell applications," *Progress in Photovoltaics: Research and Applications*, 2013.

[13] Q. Guo, G. M. Ford, R. Agrawal, and H. W. Hillhouse, "Ink formulation and low-temperature incorporation of sodium to yield 12% efficient $Cu(In,Ga)(S,Se)_2$ solar cells from sulfide nanocrystal inks," *Progress in Photovoltaics: Research and Applications*, vol. 21, pp. 64–71, 2012.

[14] J. H. Lee, J. Chang, J.-H. Cha et al., "Large-scale, surfactant-free solution syntheses of $Cu(In,Ga)(S,Se)_2$ nanocrystals for thin film solar cells," *European Journal of Inorganic Chemistry*, vol. 2011, no. 5, pp. 647–651, 2011.

[15] T. K. Todorov, O. Gunawan, T. Gokmen, and D. B. Mitzi, "Solution-processed $Cu(In, Ga)(S, Se)_2$ absorber yieldinga 15.2% efficient solar cell," *Progress in Photovoltaics: Research and Applications*, vol. 21, no. 1, pp. 82–87, 2013.

[16] Q. Guo, H. W. Hillhouse, and R. Agrawal, "Synthesis of Cu_2ZnSnS_4 nanocrystal ink and its use for solar cells," *Journal of the American Chemical Society*, vol. 131, no. 33, pp. 11672–11673, 2009.

[17] Q. Guo, S. J. Kim, M. Kar et al., "Development of $CulnSe_2$ nanocrystal and nanoring inks for low-cost solar cells," *Nano Letters*, vol. 8, no. 9, pp. 2982–2987, 2008.

[18] Joint Committee for Powder Diffraction Standards, powder diffraction file. No. 85-1575, JDCPS International Center Diffraction Data, 1997.

[19] A. Ennaoui, "Recent results on $Cu(In, Ga)(SSe)_2$ and $Cu_2(Zn, Sn)(S, Se)_4$ thin film solar cells," in *Proceedings of the 11th Symposium of Research Center for Solar Energy Chemistry Prospects for Utilization of Solar Energy: Next-Generation Solar Cells and Photocatalysts*, Osaka University, Osaka, Japan, February 2012.

[20] S. Ahn, C. Kim, J. H. Yun et al., "$CuInSe_2$ (CIS) thin film solar cells by direct coating and selenization of solution precursors," *Journal of Physical Chemistry C*, vol. 114, no. 17, pp. 8108–8113, 2010.

[21] H. Lee, W. Lee, J. Y. Kim et al., "Highly dense and crystalline $CuInSe_2$ thin films prepared by single bath electrochemical deposition," *Electrochimica Acta*, vol. 87, pp. 450–456, 2013.

[22] I. Oja, M. Nanu, A. Katerski et al., "Crystal quality studies of $CuInS_2$ films prepared by spray pyrolysis," *Thin Solid Films*, vol. 480-481, pp. 82–86, 2005.

[23] J. Eberhardt, H. Metzner, R. Goldhahn et al., "Defect-related photoluminescence of epitaxial $CuInS_2$," *Thin Solid Films*, vol. 480-481, pp. 415–418, 2005.

[24] Y. Yan, Y. Liu, L. Fang et al., "Influence of post-grown treatments on $CuInS_2$ thin films prepared by sulphurization of Cu-In films," *Rare Metals*, vol. 27, no. 5, pp. 490–495, 2008.

[25] C. Y. Cummings, G. Zoppi, I. Forbes, D. Colombara, L. M. Peter, and F. Marken, "Rocking disc electro-deposition of CuIn alloys, selenisation, and pinhole effect minimisation in CISe solar absorber layers," *Electrochimica Acta*, vol. 79, pp. 141–147, 2012.